

VARIABLE LOFT THERMAL INSULATION FOR TEMPERATURE ADAPTIVE CLOTHING

Stephen A. Fossey, US Army Natick Soldier Center
A.J. du Plessis, Midé Technology Corporation

ABSTRACT

Adaptive thermal insulation offers soldiers protection from extreme cold temperatures, while at the same time limiting overheating at warmer temperatures, without external user input. This paper presents a concept for turning adaptive thermal insulation into a reality through the use of strains induced by coefficient of thermal expansion (CTE) mismatches in bi-component fiber materials.

Bi-component polymer fibers are typically designed to minimize the differences in CTE's between the components; in this program finite element analysis (FEA) techniques were used to investigate the bi-component fiber design space to optimize the strain production from such fibers for incorporation into an adaptive thermal insulation batting. Analysis results indicate a side-by-side bi-component fiber construction is the best to induce thickness changes in a batting, provided that the interface stresses are below the material fatigue limits. Maximizing the material CTE differentials further improves batting thickness responsiveness. Thermal modeling showed that the variable loft approach is a feasible adaptive insulation concept and the system offers appreciable improvements on insulation protection over existing commercial insulation systems.

INTRODUCTION

Thermal insulation for low temperature protection can be passive, active, or adaptive in nature. Typical thermal protection systems are passive systems, i.e. with fixed levels of insulation, and layering is used to tailor the level of protection to the desired level. Layering leads to bulky, complex systems that can impede the performance of soldiers in the field. Active thermal protection systems can be tailored to provide varying levels of protection based on external adjustment. Adaptive thermal insulation automatically adjusts protection levels based on the absolute temperatures across the protection layer. The need exists for adaptive thermal protection systems that are able to provide thermal protection to soldiers over a range of temperatures with a single garment. Such an adaptive thermal protection insulation will also find wide application in the commercial outdoor, sport, rescue, and medical industrial markets.

Passive thermal insulation relies on the structure of the material to insulate with the user layering as necessary to adapt to the environment. A typical example of passive thermal insulation is Primaloft®. The designers of Primaloft® tried to mimic the macroscopic structure of down by using a mixture of thick (20 μm) fibers to provide structural integrity and stability, and thinner fibers (7.7 μm) to provide thermal efficiency. These fibers simulate the quill and branches found in down. Active thermal insulation provides the user with some level of control over the thermal

insulation of a garment during use. W.L. Gore, Inc. produces an Airvantage® variable insulation fabric based on the concept of inflatable bladders. These bladders allow user adjustment of the fabric's thermal insulation properties. The bladders are inflated by the user to provide air pockets increasing the insulation of the garment and protecting the user against body heat loss.

There are limited examples of adaptive thermal insulation in the literature. A patent by Russell et al. [1] discloses a thermally insulating textile that provides a variable degree of thermal insulation through the action of shape memory materials. In the disclosure two embodiments are covered: the first relies on a small volume change associated with the phase change in the shape memory material to produce a reversible out of plane deformation in a bulking layer; the second relies on the shape memory effect to produce large, irreversible out of plane deformations in a bulking layer. The bulking effect described in the patent aims to protect the user against high temperatures. Processing is achieved by depositing the shape memory material in a regular pattern on carrier substrates.

The focus of this development effort is an adaptive thermal insulation that relies on the combination of thermally reactive bi-component structural fibers with thin staple fibers (for thermal efficiency) to produce a thermal protection batting that changes thickness depending on the external environmental temperature. This adaptive thermal insulation is referred to as the Variloft batting (variable loft thermal insulation batting) for the rest of this paper. Different fiber cross-sectional shapes, material combinations, processing of bi-component fibers, and batting layouts can be optimized to take advantage of the effects of differential coefficients of thermal expansion (CTE) in transitioning structural fibers from a flat to a three-dimensional configuration. With the correct design, the network of fibers will produce a self-regulating fabric that gradually transitions from a flat, low loft, low thermal insulation configuration to a sufficiently high loft, high thermal insulation configuration. The basic operating principle of this adaptive thermal insulation is shown in Figure 1, in which a helically twisting bi-component fiber transitions into a three-dimensional shape from the baseline to produce the desired variable loft, depending on the external temperature. Increased thermal differentials cause the fiber to “cork” more and produce more loft.

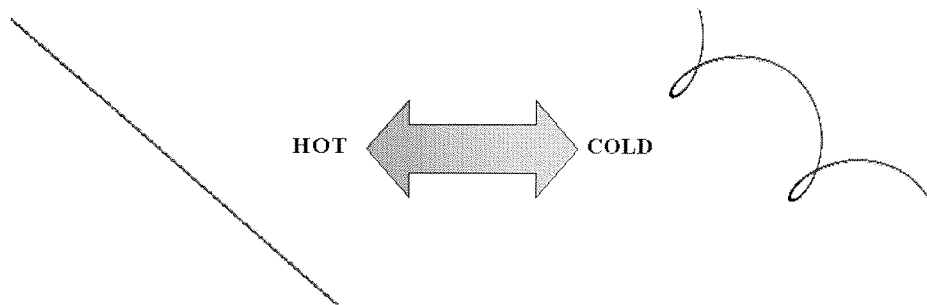


Figure 1: Variable loft, adaptive thermal insulation concept.

Development of the adaptive thermal insulation system consists of developing a detailed understanding of the mechanics of the concept through structural and thermal modeling, selection or development of a fiber material system to product thermo-reactive bi-component fibers, integrating the active fibers with thin insulating fibers into batting and finally testing of a

prototype system. This paper describes the structural and thermal modeling steps in the development of the variable loft, thermal protection batting.

OVERVIEW OF STRUCTURAL MODELING WITH THE FINITE ELEMENT METHOD

The bi-component fiber and batting structural design space were analyzed with the finite element analysis (FEA) technique using NE NASTRAN software. FEA allows the mechanical designer to analyze design alternatives for complex mechanical systems efficiently. In this specific case the focus of the analysis was to explore the impact of different geometric and material parameters on thermally induced strains in bi-component fibers as well as thickness effects on battings made from these bi-component fibers. The FEA started with a single, straight bi-component fiber, then progressed to a single, helically twisted bi-component fiber, and finally considered a non-woven batting constructed of twisted bi-component fibers. A schematic of the FEA and the design parameters considered during each part of the analysis is shown in Figure 2.

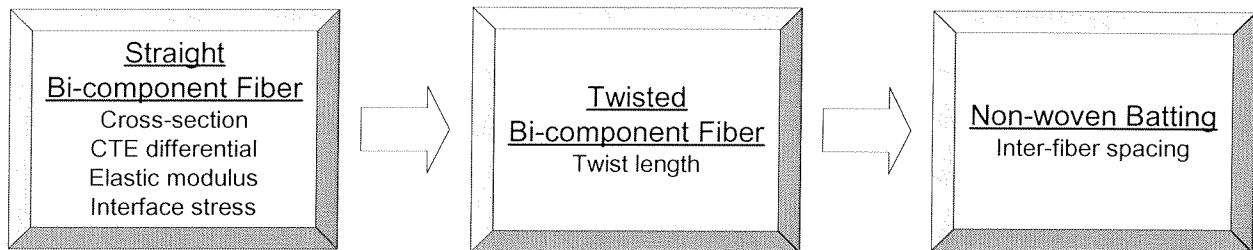


Figure 2: Adaptive thermal insulation FEA overview.

In the first part of the FEA a single, straight bi-component fiber made from two different polymers was analyzed for induced thermal strains as a function of an externally applied temperature. A convenient global measure of the induced strain in a straight fiber is the induced curvature of the fiber when subjected to the external thermal loading (assuming the fiber reacts mechanically like a long slender beam). The first design parameter analyzed was the effect of fiber cross-section on fiber curvature. From this analysis it was possible to determine the best cross-sectional configuration to maximize induced curvature. Secondly, the analysis considered the effect of material CTE differences on the induced strain. As the CTE difference of the component materials increase, the thermal straining force increases and as a result the curvature should increase. One additional material parameter analyzed was the elastic stiffness of the bi-component fiber materials. If one material is very stiff compared to the other induced fiber curvature is not expected. This is subject to the specific fiber cross-section. Finally, the interfacial stresses were analyzed in the last step of the straight fiber analysis. There is a large stress gradient across the interface boundary in the bi-component fiber and the analysis aimed to quantify the typical stress levels expected. This is important to ensure the fibers will not split during temperature induced bending.

In the next step of the FEA a twisted bi-component fiber was analyzed. The only difference between the straight and twisted bi-component fiber is the addition of helical twist along the length of the fiber. Helical twist causes the fiber to curl up like a corkscrew as the temperature is reduced and this curling produces a thickness change in a batting. The effect of twist length (or

period) on the curl diameter was investigated in this part of the FEA. Finally, the non-woven batting made from twisted bi-component fibers was analyzed to quantify the effect of inter-fiber spacing (effectively batting density) on batting thickness. Results from the FEA was used to make design recommendations for the prototype batting.

STRAIGHT BI-COMPONENT FIBER ANALYSIS

Straight fiber model

The single straight fiber model is based on a straight, solid fiber of the various cross-sections seen in Figure 3 (All fibers have a 50/50 area ratio for each material). Each fiber cross-section has the equivalent area of a 0.025 mm diameter fiber. Table 1 shows the distance between the centroids of each “half” of the fiber cross-sections. Figure 4 shows the isometric view of the Fiber 3 straight fiber solid model. The fiber was modeled with beam elements 0.1 mm long with 10 elements along the length. In the model the one end of the fiber was fixed while the other was left free.

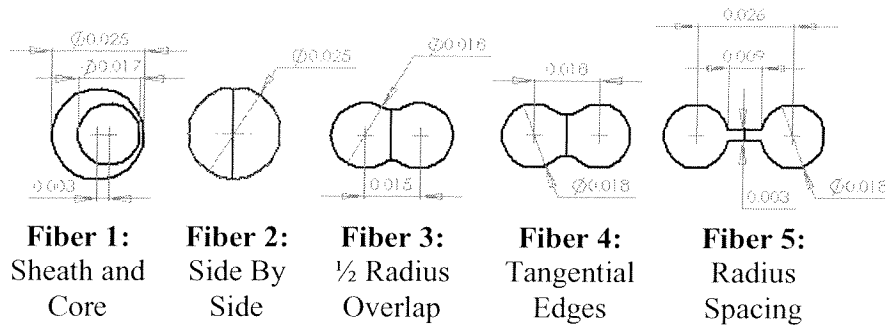


Figure 3: Bi-component fiber cross-sections for FEA (dimensions in mm).

Table 1: Fiber cross-section centroid offsets.

Fiber	Centroidal distance (mm)
1	0.0055
2	0.0106
3	0.0155
4	0.0175
5	0.026

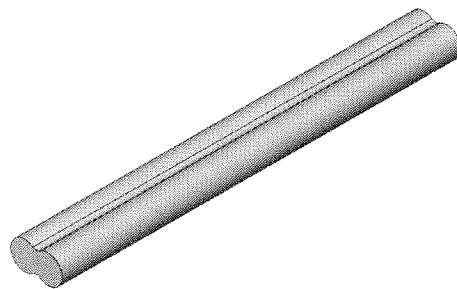


Figure 4: Fiber 3 straight fiber solid model.

Two different materials were specified for the fiber components. Baseline mechanical and thermal properties of the materials are listed in Table 2. Material 1 is based on Nylon 6 and Material 2 is based on Nylon 6 PA 6. The baseline coefficients of thermal expansion are based on the goal values for the materials development task of the project.

Table 2: Fiber material mechanical properties.

Properties	Material 1	Material 2
Elastic Modulus (GPa)	1900	1200
Poison's Ratio	0.33	0.33
Yield Strength (MPa)	62.4	25
CTE (m/m°C)	1x10e-6	250x10e-6

Effect of fiber cross-section on curvature

The single straight fiber model was used to determine curvature of the straight fibers using a 60 °C temperature differential. Curvature of the fiber is determined by the following formula:

$$C = \frac{1}{R} \quad (1)$$

with

C = fiber curvature, and

R = fiber bending radius.

Therefore, determining the radius of the fiber curve, the curvature is also determined. The radius for the various fibers was determined using a base node and a tip node. The undeformed node location and the translations experienced by the tip node were used to determine the radius. Figure 5 illustrates the method used to determine the radius values.

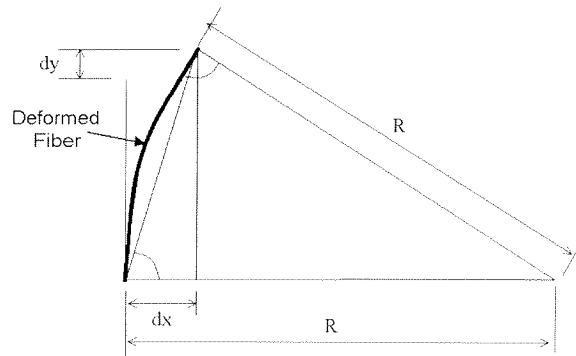


Figure 5: Curvature calculation illustration.

$$\alpha = \tan^{-1} \left(\frac{y + dy}{dx} \right) \quad (2)$$

$$\beta = 180 - 2\alpha \quad (3)$$

$$R = \frac{y + dy}{\sin \beta} \quad (4)$$

Figure 6 shows the results of the NASTRAN model curvature analysis. The curvature of the fibers shown is for a CTE differential of $249 \mu\text{m}/\text{m}^\circ\text{C}$. Fiber 2 (0.0106 mm centroidal distance), the side-by-side fiber, produces the highest level of induced curvature.

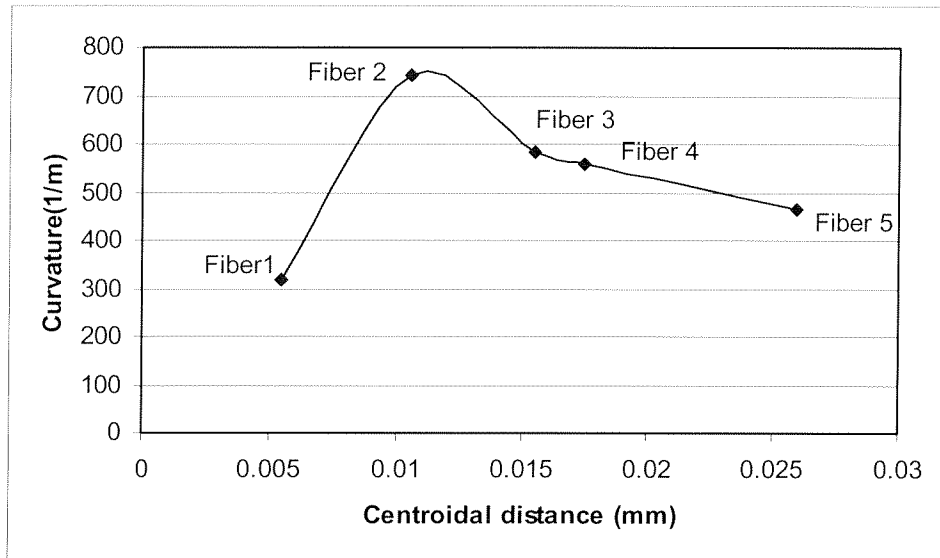


Figure 6: Cross-sectional effect on curvature for $249 \mu\text{m}/\text{m}^\circ\text{C}$ CTE differential.

Effect of CTE differential on fiber curvature

The effect of CTE differential on curvature was examined using the single, straight fiber model for Fiber 3 (Fiber 3 was initially selected as the baseline cross-section for all analysis). Table 3 shows the CTE values used for the analysis. All other parameters were maintained at the baseline levels. Figure 7 shows the effect of the CTE differentials on the straight fiber model for Fiber 3. This analysis confirmed initial assumptions that the larger the CTE differential, the greater the fiber deformation. The CTE differential effects the curvature in a linear fashion. Additionally it is only the CTE differential that is important, and not the absolute values of the material CTE's.

Table 3: Coefficient of thermal expansion (CTE) variations for NASTRAN Model.

Material 1 – CTE ($\mu\text{m}/\text{m}^\circ\text{C}$)	Material 2 – CTE ($\mu\text{m}/\text{m}^\circ\text{C}$)	CTE Differential ($\mu\text{m}/\text{m}^\circ\text{C}$)
1.0	150	149
50	150	100
100	150	50
1.0	200	199
50	200	150
100	200	100
1.0	250	249
50	250	200
100	250	150

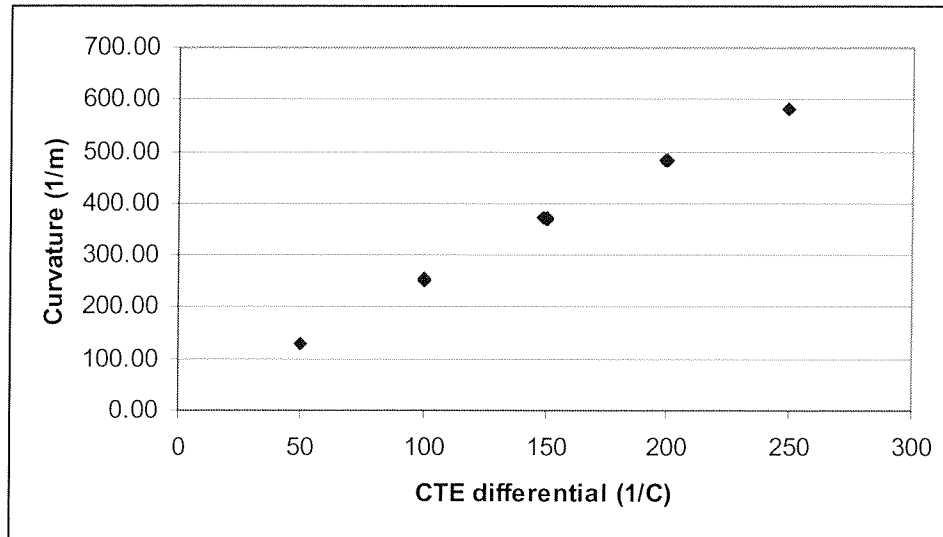


Figure 7: Effect of CTE differential for Fiber 3.

Effect of material elastic moduli ratio on induced fiber curvature

The curvature of the single straight bi-component fiber was analyzed for a range of different material elastic moduli ratios between the component materials to determine the effect it has on induced fiber curvature. Applied external thermal loading was maintained at 60°C and the CTE differential was set at the baseline value of 249 $\mu\text{m}/\text{m}^\circ\text{C}$. Table 4 lists the elastic moduli used in this analysis.

Table 4: Elastic modulus ratios.

Elastic Modulus Ratio (E_2/E_1)	E_1 (MPa)	E_2 (MPa)
0.25	1900	475
0.5	1900	950
0.63	1900	1200
0.75	1900	1425
1.0	1900	1900
1.3	1425	1900
1.583	1200	1900
2.0	950	1900
4.0	475	1900

Figure 8 shows the results of the modulus analysis. While slight variations in the curvature plots are evident, the conclusion is that overall, the effect of elastic modulus differences are limited and in general can be ignored for a given fiber cross-section.

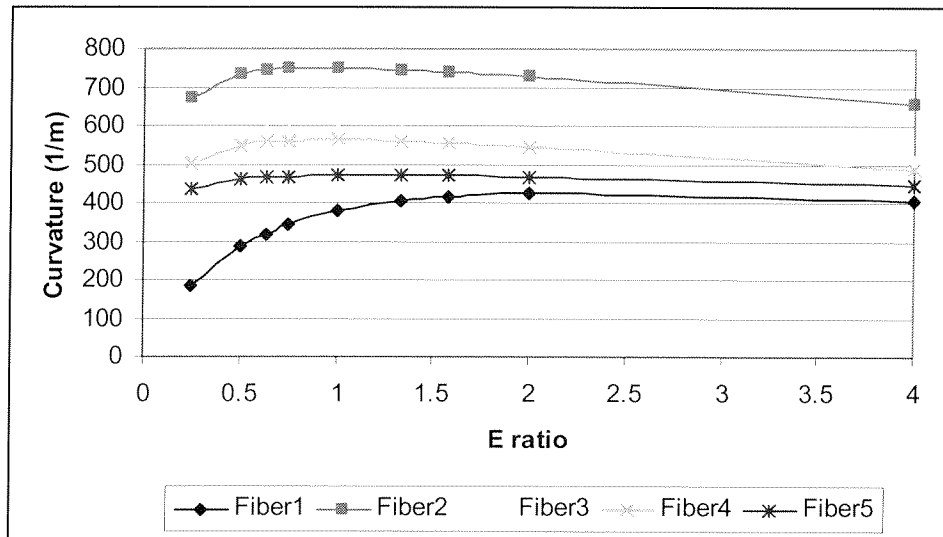


Figure 8: Elastic modulus ratio effect on the curvature of various fiber cross-sections.

Stresses at the material interface for bi-component fibers

A solid element model of the different fibers was used for the stress analysis. The model analyzed the effects of varying the CTE of the component materials and the different fiber cross-sections on the stress in the fiber, under a 60 °C thermal loading. Baseline material properties were used for the fiber materials. Table 5 shows the maximum von Mises stresses on the fiber cross-sections for a CTE differential of 249 $\mu\text{m}/\text{m}^\circ\text{C}$.

Table 5: Maximum von Mises stress for CTE differential of 249 $\mu\text{m}/\text{m}^\circ\text{C}$.

Fiber	Maximum von Mises stress (MPa)
1	46.6
2	27.7
3	27.1
4	25.7
5	19.1

The maximum stress occurs, as expected, in the area of the material property discontinuity between the two fiber materials. Interfacial von Mises stresses in the majority of the fibers are higher than the yield strength of Material 2, 25 MPa, the less strong of the two materials. Excessive stresses can lead to plastic deformation of the bi-component fiber or fatigue of the fiber during thermal cycling. Future fiber designs should address this over-stressing issue for a practical adaptive thermal insulation.

HELICAL BI-COMPONENT FIBER ANALYSIS

The single fiber helical model is comprised of beam and rigid elements as seen in Figure 9. The straight fiber is referred to as the main fiber and the helical or wrap fiber is rotated around the main fiber. The two fibers are connected using rigid elements to simulate the adhesion between the two components of each fiber.

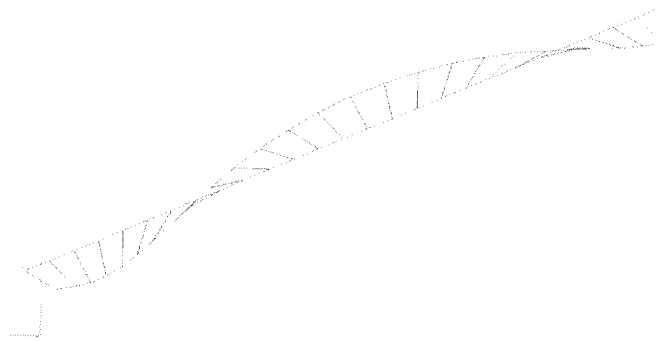


Figure 9: Helical Fiber Construction.

The wrap fiber was adjusted to accommodate the various fiber cross-section center points. Each cross-section was applied using the beam element's properties. The helical elements were rotated in the model to maintain the approximate twist of the actual fiber to preserve a consistent overall cross-sectional shape. The fiber was analyzed for a 2 mm, 3 mm, and 4 mm helical twist and was 10 mm in length. As with the straight fiber model, one end of the fiber was fixed and the other end was free for the analysis. A deformed single fiber helical model is shown in Figure 10.

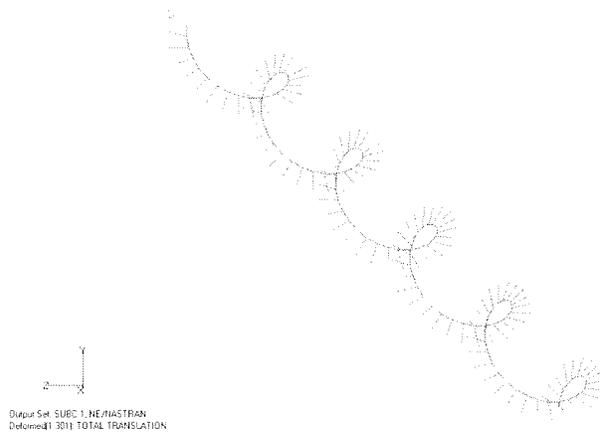


Figure 10: Deformed single fiber helical model.

Figure 11 shows the diameter that is used to determine the effect of twist length for a given CTE differential and fiber cross-section. Radius of the deformed helical fiber was determined from the nodal displacements in the y-z plane. Results for each cross-section and helical twist length are shown in Figure 12, indicating that Fiber 2 provides the best helical radial change. Included in the results are the curvature results from the straight fiber analysis. The twisted fiber radial results show the same trend as the curvature results for the single straight fiber.

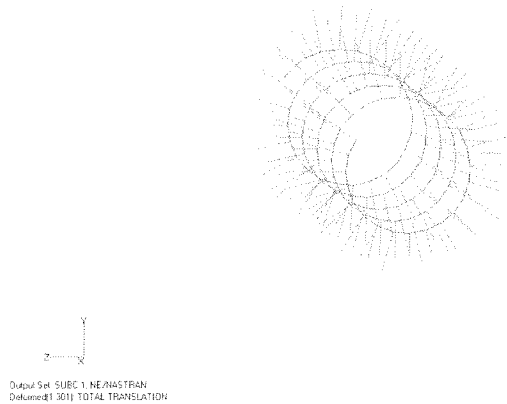


Figure 11: Diameter view of deformed single fiber helical model.

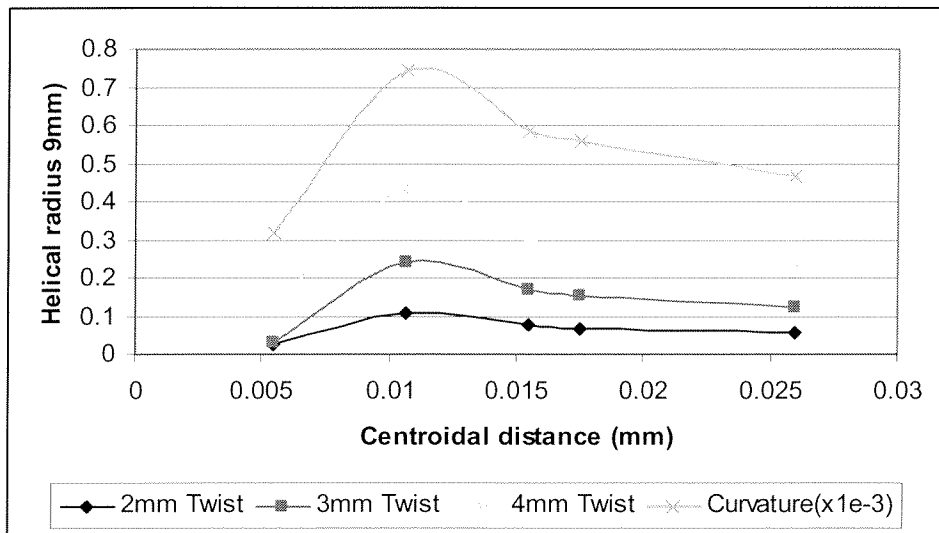


Figure 12: Radius data summary for a CTE differential of $249 \mu\text{m}/\text{m}^\circ\text{C}$.

From the single fiber FEA results is clear that Fiber 2, the side-by-side bi-component fiber construction has the greatest deformation for a given CTE differential. In addition, the larger the CTE differential and greater the helical twist length, the greater the fiber deformation.

NON-WOVEN BATTING ANALYSIS

Finally, a non-woven batting model was constructed based on the single fiber helical model. The non-woven batting model was used to analyze the effect of fiber spacing on batting thickness and to determine the thickness of the baseline batting (batting made from baseline materials and with a twist length of 2 mm). Eight layers of bi-component fibers comprise the model. The fibers of each layer were shifted along their lengths to provide randomness for each fiber layer in the batting. This shift can be seen in the fibers shown in Figure 13. This shift simulates the random nature of a non-woven batting. Each layer was rotated 90 degrees to the orientation of the

previous layer to further simulate a real batting. While the model does still have a regular pattern, it is believed that it will provide a good estimate of batting performance.



Figure 13: Shifting of fibers for batting randomness.

The *inter-fiber* spacing, or spacing between the centerline of each *fiber* on the same layer, was varied to determine the effect of the inter-fiber spacing on the batting thickness changes. Spacings of $\frac{1}{2}$ mm, 1 mm, 2 mm and 4 mm were analyzed. The *inter-layer* spacing, or spacing between the centerline of each *fiber layer*, is 0.025 mm. Figure 14 shows the inter-fiber and inter-layer spacing. The fibers of each layer running in the same direction were shifted to have a horizontal spacing of half the inter-fiber spacing. Fiber 1 and fiber 2 of Figure 14 illustrate this horizontal spacing.

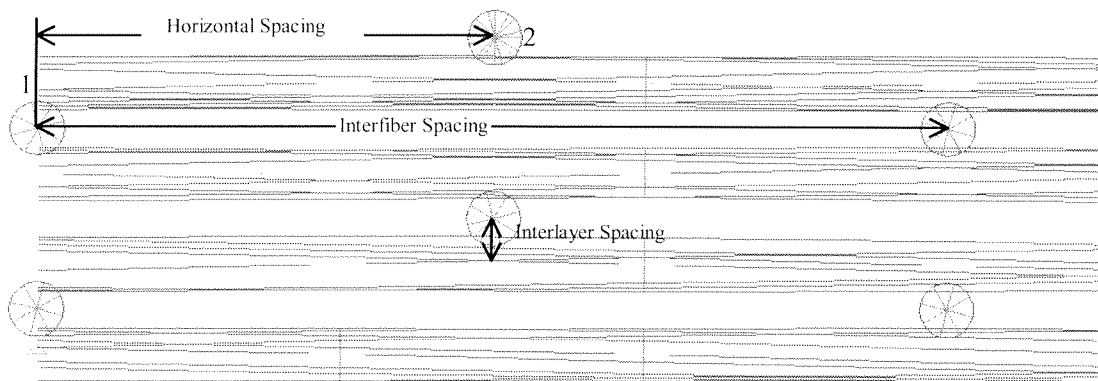


Figure 14: Inter-fiber and inter-layer spacing of the NASTRAN fiber model.

Between each layer, the points where the fibers cross were joined with rigid elements to simulate the adhesion between the fibers to form the non-woven batting. Displacement constraints for the analysis were placed on the 4 corners of the batting model. One corner was fixed in x, y, and z, one fixed in x and y, one fixed in y and z, and the last corner was fixed in y. The batting was aligned so that the thickness of the batting was in the y-direction. The initial batting thickness from centerline to centerline of the top and bottom fibers was 0.175 mm (8 layers at 0.025 mm spacing from center to center).

The different fiber cross-sections were then analyzed for different inter-fiber spacings, using the CTE differential of $249 \mu\text{m}/\text{m}^\circ\text{C}$, a fixed helical twist length of 2 mm, and a 60°C thermal loading. Figure 15 shows the resulting batting thickness for each cross-sectional shape and inter-fiber spacing.

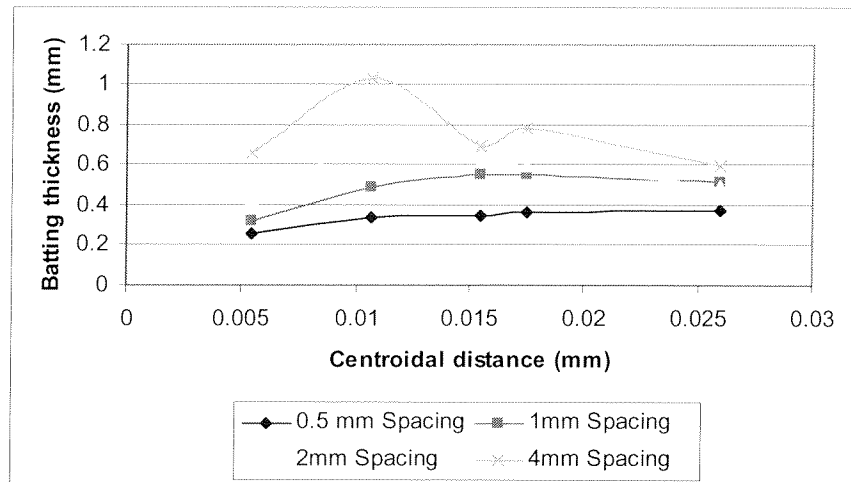


Figure 15: Batting thickness for varying fiber cross-sections and inter-fiber spacing with 2mm twist fibers.

The same batting thickness analysis was repeated using fibers with a helical twist length of 4 mm instead of 2 mm. Figure 16 shows the resulting batting thickness for each cross-sectional shape and inter-fiber spacing. For the batting made from 4 mm twisted, side-by-side fibers with an inter-spacing of 4 mm the total batting thickness is 2.25 mm as compared to 1.03 mm for the batting made of 2 mm twisted fibers under the same 60 °C thermal loading. Therefore, it is clear that a batting made from fibers with the longest twist and the largest inter-fiber spacing produces the best batting thickness gain.

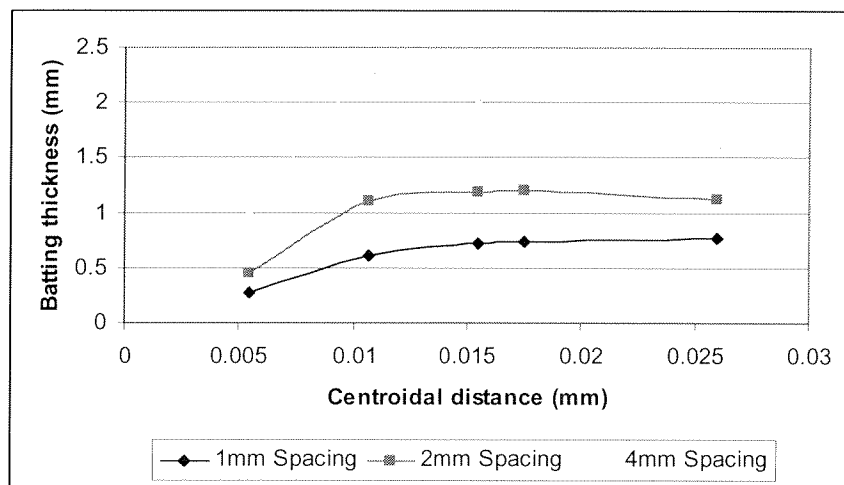


Figure 16: Batting thickness for varying fiber cross-sections and inter-fiber spacing with 4 mm twist fibers.

ADAPTIVE THERMAL INSULATION MODELING

A thermal model was developed to evaluate the effectiveness of the Variloft batting at providing adaptive thermal insulation. The batting is assumed to consist of two subcomponents for thermal modeling purposes. This two-subcomponent structure replicates the structure of natural down and artificial Primaloft® (previously described): thick structural fibers (~ 25 μm) supporting thin

(~7 μm) thermally efficient fibers. The structural fibers provide bulk to the batting. The bulk, in turn, provides the air layer contributing to the insulation provided by the batting by virtue of the conduction of heat through the air layer. The thin fibers prevent any local convection heat transfer in the batting and reduce the level of radiation heat transfer through the batting. Based on these assumptions the rate of heat transfer through the batting is the sum of the conductive heat transfer and the radiative heat transfer:

$$q_{tot} = q_{cond} + q_{rad} = \frac{k_{eff} A (T_i - T_o)}{t_{bat}} + \epsilon_{eff} \sigma A (T_i^4 - T_o^4) \quad (5)$$

with

- A = Batting area [m^2],
- ϵ_{eff} = effective batting emissivity,
- k_{eff} = effective conductive heat transfer coefficient of batting area [W/mK],
- q = heat transfer [W],
- $T_{i,o}$ = batting boundary temperatures on the inside and outside of batting [K],
- t_{bat} = thickness of batting [m], and
- σ = Stefan-Boltzmann constant [$\text{W/K}^4\text{m}^2$].

Stuart and Holcombe [2] showed that the heat transfer through a low fiber volume fraction thermal insulation batting could be approximated with:

$$\frac{q_{tot}}{A} = \left(\frac{k_a}{x} + I \right) (T_i - T_o) \quad (6)$$

with

- I = effective radiation heat transfer constant [W/Km^2], and
- k_a = thermal conductivity of air [W/mK].

For a given batting system the effective radiation heat transfer constant is constant with batting thickness, but varies with the ambient external temperature as well as the difference between the internal and the external temperatures. Based on experimental testing by Farnworth [3], the radiation constant for Thinsulate® at an ambient temperature of 300K has been determined to be 0.21 W/Km^2 . The fiber diameter of Thinsulate® at 3 μm were assumed an acceptable match to the 7 μm diameter of the thermally efficient fibers envisaged for use in the Variloft batting and based on this fact the radiation constant for the current thermal model was set at 0.21 W/Km^2 . Thinsulate® is an efficient thermal radiation barrier due to small fiber size and relatively high density, therefore the use of 0.21 W/Km^2 for the radiation constant probably understates the radiant heat transfer to be expected from the proposed material.

The thickness of the Variloft batting is the sum of the thicknesses of each of the structural sub-layers in the batting. Sub-layer thickness depends on the temperature of the specific layer, which is a function of the temperature distribution through the batting. Batting thickness can be expressed as:

$$t_{bat} = \sum_n t_1(T_1) + t_1(T_1) + \dots + t_m(T_m) \quad (7)$$

with

$T_{1,2,m}$ = layer mean temperature [K], and

$t_{bat,1,2}$ = batting and layer thicknesses [m].

The advantage of using discrete sub-layers to represent a batting is to simplify the process of modeling a batting where the sub-layers are made from different materials and have different thickness responses. To solve for the batting thickness a temperature distribution is assumed. Based on this temperature distribution, the mean layer temperature and layer thicknesses are determined. Layer thicknesses are added to determine the new batting thickness and this thickness is used to determine a new temperature distribution. This iterative process is repeated until the batting thickness converges. Once the batting thickness is determined, the batting thermal resistance value, R , the clo value, and the clo mass efficiency can be determined from:

$$\frac{1}{R} = \frac{q_{tot}}{A(T_i - T_o)} = \left(\frac{k_a}{x} + I \right) \quad (8)$$

and

$$clo = \frac{R}{0.155} \quad (9)$$

The thermal model was used to determine the insulation offered by a Variloft batting, assuming a batting with the same density as Primaloft®, 0.18 kg/m² (5.3 oz/yd²), a 15% structural fiber volume, 23 layers of adaptive structural fiber with the thickness of the layer linearly dependant on the layer mean temperature. The individual layer thickness is based on the results of the FEA model for the non-woven batting assuming a 249 µm/m°C CTE differential for the components of the 4 mm twist bi-component fibers, with an inter-fiber spacing of 4mm. For the model it is assumed that the layers are flat at 45°C, the maximum operating temperature where insulation should be minimized to prevent overheating. All the input parameters for the thermal model are given in Table 6:

Table 6: Variloft thermal model parameters.

Parameter	Value/Function
Batting areal density	0.18 kg/m ²
Structural fiber volume	15%
Individual layer thickness	$t(T) = -0.000035T + 0.00159$ m (T in °C)
Number of layers	23
Internal temperature	30 °C
External temperature	-45 °C to 15 °C
Air conductivity	0.026 W/m°C
Radiation parameter, I	0.21 W/°Cm ²

The properties of Primaloft®, down, and Polargard® are from two previous studies [4,5] of insulation materials and should be taken as indicative of the properties of typical fibrous insulation materials rather than definitive measures of commercial materials. Batting thickness over the range of external temperatures is shown in Figure 17. The change in Variloft batting thickness with temperature is less pronounced than the change in a single layer thickness due to the fact that fiber layers next to the human body are at a higher mean temperature than layers on the outside. Figure 18 and Figure 19 show the insulation protection, expressed in clo, and the thermal insulation mass efficiency of the Variloft batting for the assumed construction. The calculated thermal protection of the Variloft batting is 54% better than the next best commercial system, Primaloft®, at -45 °C; however, that value should be viewed with caution because the radiant heat transfer coefficient probably over estimates the insulation offered by Variloft as mentioned previously.

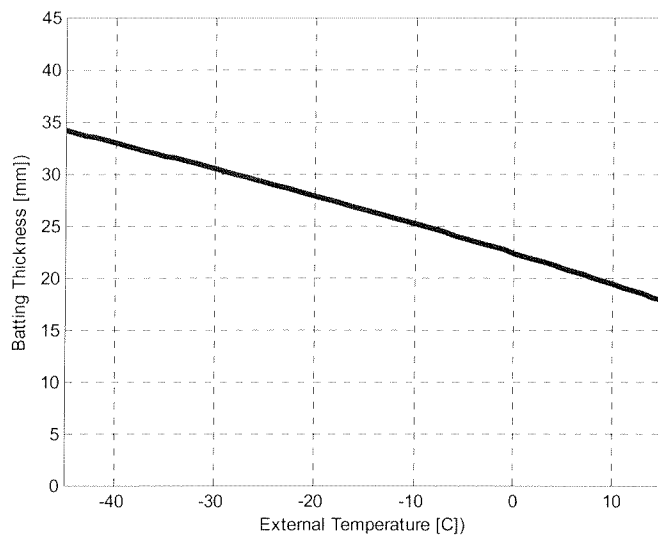


Figure 17: Variloft batting thickness.

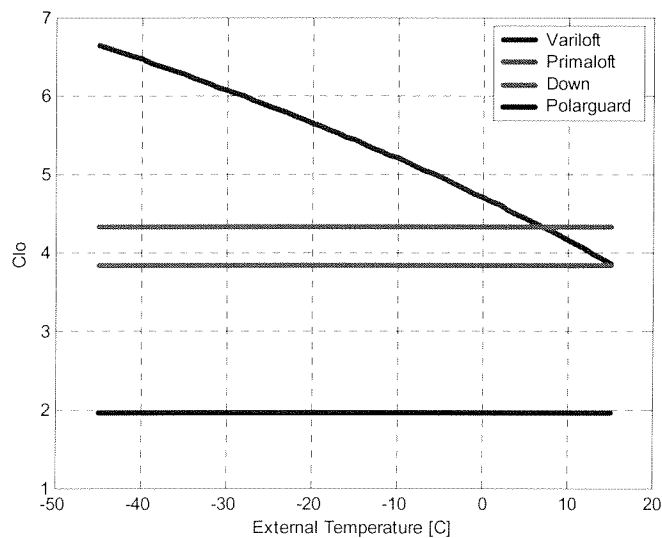


Figure 18: Variloft insulation protection.

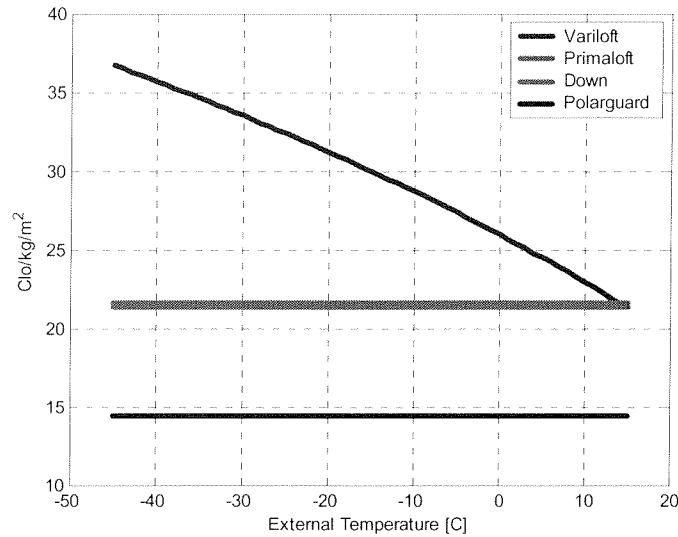


Figure 19: Variloft insulation protection mass efficiency.

SYSTEM PERFORMANCE REQUIREMENTS

The thermal balance of a soldier in the field is a complex situation involving not only the loss of heat by conduction, convection, and radiation to the environment, but also heat gain from solar loading and variable heat production by the individual. Heat balance based on changing work rates is predominantly maintained by changes in sweating rate but there are also changes in internal temperature in cold environments. At the present time soldiers are expected to respond to changes in the environment, on a day-to-day basis or during a day, by opening vents or removing layers. While this approach is effective it leads to the need for a number of different garments to adapt to different conditions and since it is often inconvenient to remove layers overheating and subsequent sweating lead to moisture build-up in insulation and increased water requirements. A thermally adaptive insulation can compensate for some or all of the changes in the thermal environment automatically.

A full analysis of the thermal balance of a soldier is beyond the scope of this paper, but given the importance of the problem considerable work has already been done. Santee [6] has provided an overview of simple models that require only a skin temperature and an ambient temperature to predict the level of insulation required to maintain heat balance for a person at rest (sitting). Equation (10) is that of Burton and Edholm [7] as reported in Santee [6] without sweating heat loss.

$$I = 0.112(33 - T_a) / M \quad (10)$$

where I is the insulation required in clo, T_a is the ambient temperature in degrees C, and M is the work rate in MET units (a sitting person generates 1 MET of energy or about 105 watts). Figure 20 shows a plot of required insulation, the calculated performance of Variloft and that of Primaloft® as a function of temperature. The temperature range depicted in Figure 20 ranges

from a comfortable room temperature to an arctic winter temperature. While the Variloft does not completely compensate for environmental changes it clearly extends the window of temperatures over which the insulation compensates. It is different in kind from conventional insulations as represented by Primaloft®, a state-of-the-art non-adaptive thermal clothing insulation.

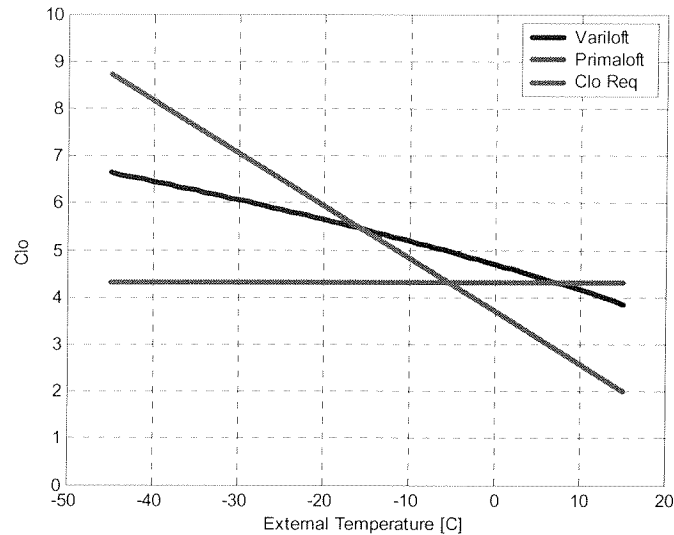


Figure 20: Insulation provided vs. insulation required.

CONCLUSION

Adaptive thermal insulation offers soldiers in the field protection from extreme cold temperatures, while at the same time limiting any overheating at warmer temperatures, without any external user input. This paper presented a concept for turning the idea of adaptive thermal insulation into a reality through the use of thermally driven bi-component fiber straining based on component material CTE mismatches. The Variloft batting concept results in a self-regulating, insulation batting that transforms from a flat structure at high temperatures into a thick, 3-dimensional structure at low temperatures.

FEA techniques were used to investigate the bi-component fiber design space to optimize the strain production from such fibers for incorporation into an adaptive thermal insulation. Analysis results indicate the side-by-side bi-component fiber construction is the best, provided that the interface stresses are below the material fatigue limits. To maximize batting thickness the material CTE differential should be maximized. Fiber twist and layer density does affect the batting thickness, but these parameters is largely controlled by the processing techniques used to produce the insulation batting. Thermal modeling showed that the Variloft system is a feasible adaptive insulation concept and the system offers appreciable improvements on insulation protection over existing commercial insulation systems.

The next task in this program is to move the concept from the design stage into the laboratory by completing the fiber material development. In order to make the Variloft batting a reality a set of

polymer materials must be identified that are compatible for processing but at the same time exhibit large differences in the CTE characteristics when spin into bi-component fibers.

REFERENCES

1. Russell; D.A., Elton; S.F., Congalton; D., "Thermally insulating textile", US. Patent No. 6,312,784.
2. Stuart, I.M., and Holcombe, B.V., "Heat Transfer Through Fiber Beds by Radiation with Shading and Conduction", Textile Research Journal, Vol. 54, 1984, pp 149-157.
3. Farnworth, B., "Mechanisms of Heat Flow Through Clothing Insulation", Textile Research Journal, Vol. 53, 1983, pp 717 – 724.
4. Dent, R. W., Donovan, J. G., Skelton, J., and Fossey, S. "Development of Synthetic Down Alternatives", Natick/TR-86/021L, April 1984.
5. Dent, R. W., Donovan, J. G., Skelton, J., and Fossey, S. "Development of Synthetic Down Alternatives Phase II", Natick/TR-87/004L, January 1986.
6. Santee, W. R. "A Simplified Modeling Approach for Estimating Heat Loss during Cold Exposure" U. S. Army Research Institute of Environmental Medicine Report 19960805 091, June 1996.
7. Burton, A. C. and Edholm, O. G., "Man in a Cold Environment: Physiology and Pathology Effects of Exposures to Low Temperatures", E. A. Arnold, London 1955.

ACKNOWLEDGEMENT

This research and development program is funded by the US Army Solder Systems Center under Contract No. W911QY-04-C-0010.

Contact details of the authors are:

Stephen A. Fossey
US Army Natick Soldier Center
15 Kansas Street
Natick, MA 01760-5020 USA
[REDACTED]

A. J. du Plessis
Midé Technology Corporation
200 Boston Ave, Suite 1000
Medford, MA 02155 USA
[REDACTED]